PHYSICAL REVIEW B **81**, 075411 (2010)

Low-energy ion-induced electron emission in metal-insulator-metal sandwich structures

Domocos Kovacs
Experimentalphysik II, Ruhr-Universität Bochum, 44801 Bochum, Germany

Artur Golczewski, Gregor Kowarik, and Friedrich Aumayr
Institut für Allgemeine Physik, Technische Universität Wien, A-1040 Vienna, Austria

Detlef Diesing
Physikalische Chemie, Universität Duisburg-Essen, 45117 Essen, Germany

(Received 26 June 2009; revised manuscript received 12 November 2009; published 9 February 2010)

An Ag-AlO_x-Al sandwich structure is used to investigate the electronic excitation induced by Ar^+ ions at the surface of the top 15 nm Ag film. The internal electron emission yield, i.e., the number of electrons emitted per impinging ion into the bottom Al film, is determined as a function of the kinetic energy of the ions in the range of 300–6000 eV. A comparison to the external electron emission yield, i.e., the number of electrons per projectile ejected into the vacuum, reveals two interesting aspects. First, unlike in the external emission, no significant contribution of the potential energy to the internal electron emission yield is observed. Second, the kinetic part of the electron emission yield exceeds the external one over the entire energy range. Another interesting result is that the internal emission yield shows a power-law dependence on ion kinetic energy. A Monte Carlo simulation, based on a simple theoretical treatment of the kinetically induced electron emission, supports the experimental findings. Finally, we discuss the influence of excitation properties (e.g., anisotropy) as well as of device properties (e.g., film thickness, barrier height) on the computed electron emission yields.

DOI: 10.1103/PhysRevB.81.075411 PACS number(s): 79.20.Rf, 41.75.Ak, 73.40.Rw, 07.77.Ka

I. INTRODUCTION

It is known for a long time[1] that the bombardment of a solid with ionic projectiles leads to the ejection of electrons from the surface. In the last century, the phenomenon was intensively investigated and a vast number of papers and reviews has been dedicated to this subject.[2,3] The basic features of this ion-induced electron emission (EE) are well understood: upon ion-surface collision, the energy carried by the projectile is dissipated within the solid. This causes the excitation of target but also of projectile electrons which then undergo a cascade of elastic and inelastic collisions, leading to further electronic excitations. Some of the excited electrons which are directed toward the surface can escape and give rise to the so-called secondary electron emission. Nevertheless, much work had to be done in order to clarify the underlying excitation mechanisms.

Since ions carry potential as well as kinetic energy, it was first differentiated between potential and kinetic electron emission. While the mechanism of potential electron emission (PEE) was already explained in early years[4–6] to be based on elementary Auger ionization processes, there is an ongoing debate on the mechanisms governing the kinetic electron emission (KEE), especially at low velocities ($v < 1$ a.u.). The first theory on KEE at low kinetic energies was proposed by Parilis and Kishinevskii[7] who suggested the electron emission to be mainly the result of an Auger recombination of a conduction electron with a core-level hole. The theory is based on an energy-transfer mechanism similar to that of Firsov[8] and shows a good agreement with the experimental results. It was demonstrated[9] that this could not be the only excitation mechanism and that, instead, the direct binary collisions between the projectile and the target valence-band electrons are primarily responsible for the KEE induced by light ions on metal surfaces.[10]

The binary collision approach successfully predicted the existence of a threshold impact velocity v_{th} (Ref. 10) under which no EE should occur, as shown in experiments with light projectiles such as H or He.[10,11] It proved to be, however, insufficient in explaining scattering results with heavier projectiles.[12] Being highly inefficient in exciting free electrons above the vacuum barrier, the binary collision theory predicted a v_{th} which was too high, since EE was observed in experiments with rare-gas[11] and metal ions[13] even below this threshold. As a consequence, the so-called "electron promotion" (Ref. 14) has been proposed[15] as a second important mechanism at low energies. Here, the electrons are promoted in higher-energy states as a result of a close collision of the projectile with target atom cores.

While most of the literature on KEE refers to electrons emitted into the vacuum, it has been shown recently[16–19] that the ion-induced EE can also be investigated by employing a metal-insulator-metal (MIM) sandwich structure as a target. In this approach, the electrons excited in the top-metal film can be detected in the bottom-metal film as an internal EE current after passing the internal potential barrier provided by the thin oxide layer. This method is, hence, suitable to investigate the transport of excited electrons in thin metal films and may provide complementary information on the ion-induced electronic excitation. Since excited electrons in such MIM systems may be emitted both into the vacuum and the bottom metal, we will distinguish correspondingly between *external* and *internal* electron emission.

In the present paper, we report on the internal and the external electron emission induced by low-energy ($E_{kin} < 6$ keV) singly-charged argon ions in a thin-film Ag-AlO_x-Al structure. We will show that the relatively high internal yields compared to the external ones, as found in the experiments, can be explained within a Monte Carlo (MC)

 ©2010 The American Physical Society

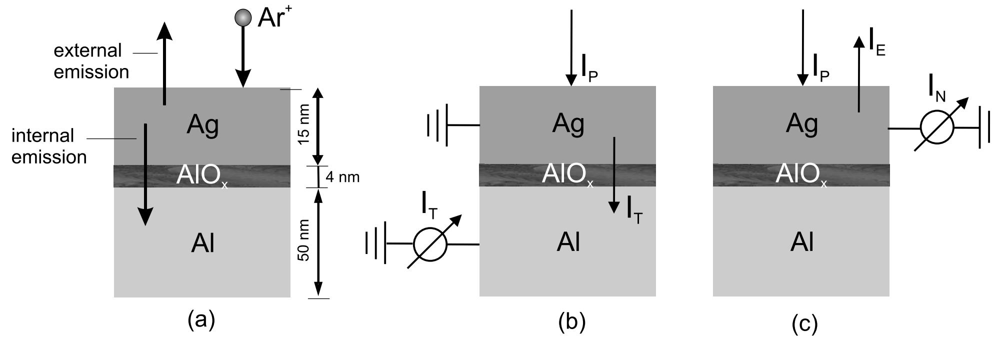

FIG. 1. (a) Schematic drawing of the Ag-AlO$_x$-Al thin-film tunnel junction, with the silver face being bombarded by singly-charged argon ions. Sketch illustrating the measurement of the (b) internal and (c) external electron emission currents, respectively.

simulation based on a model which includes the transport through a free-electron gas and the emission of excited electrons into the vacuum and over the internal barrier, respectively.

II. EXPERIMENT

A sketch of a typical metal-insulator-metal junction employed in our experiments is shown in Fig. 1. The samples have been obtained by the evaporation of 50 nm aluminum onto an insulating glass substrate, followed by a local anodic oxidation of the aluminum film to form an about 4 nm aluminum oxide layer, and finally by the evaporation of about 15 nm silver on top. Further details on the preparation procedure can be found in Refs. 20 and 21. All experiments were performed under high-vacuum conditions (base pressure of typically $p=2\times10^{-8}$ mbar). The samples were irradiated under normal incidence with singly-charged Ar^+ ions produced by an ECR ion source of 14.5 GHz described in detail in Ref. 22. The ion beam was operated in a pulsed mode with a typical pulse width of 1.5 s. In the range between 1 and 6 keV, the kinetic energy of the argon ions was set by varying source potential between +1 and +6 kV, while below 1 keV it was set by keeping the source potential constant at +1 kV and by applying a retarding field to the sample and a deceleration lens in front of it to slow down the ions. Under the applied conditions, no changes of the current-voltage characteristics of the tunnel junction have been observed during the experiments.

In the present work, both the internal and the external electron emission have been investigated. The internal electron emission is characterized by the EE yield γ_i, which is defined as the net number of electrons per impinging ion flowing across the oxide barrier and detected in the bottom aluminum film, while the external electron emission is characterized by the EE yield γ_e, defined as the number of electrons per impinging ion ejected into the vacuum.

For the case of singly-charged ions, γ_i is defined as $\gamma_i = I_T/I_P$, where I_T is the electron current flowing across the oxide layer during ion bombardment (tunneling current) and I_P is the primary ion-beam current [see Fig. 1(b)]. I_T was measured directly in the aluminum electrode by grounding the silver electrode, being recorded as a voltage signal by means of a current-to-voltage converter with a conversion factor of 10 mV/pA. It is positive when a net number of electrons is flowing from the silver into the aluminum electrode.

The external emission yield can be expressed as $\gamma_e = I_E/I_P$, where I_E is the external electron emission current, i.e., the number of electrons ejected per unit time into the vacuum times the electron charge. γ_e was determined in two independent ways: (i) by measuring the neutralization current I_N using the circuit sketched in Fig. 1(c), where I_P was measured on a Faraday-Cup mounted just below the sample, and (ii) from a polycrystalline silver foil by a current method with a retardation grid as described in details in Ref. 23. The results obtained with the latter method proved to be more accurate and will be therefore those discussed in this paper.

III. MONTE CARLO SIMULATION

An analysis of the electron transport in solids can be carried out either by solving a set of Boltzmann transport equations[24] or within a simple ballistic model as used in the description of ballistic electron emission microscopy (BEEM) data.[25] The former approach is normally employed when the mean-free path (MFP) of electrons is small compared to the film thickness d, being extremely time-consuming, while the latter is only appropriate when the MFP is comparable or larger than d, having the disadvantage of neglecting the excitation of secondary electrons in subsequent electron-electron scattering processes.

According to the theory of Fermi liquids,[26] the MFP for electron-electron scattering in metals is larger than our film thickness of 15 nm at excess energies of a few eV. This inelastic MFP decreases with increasing energy, showing a minimum of roughly 1 nm at energies of about 40 eV.[27] Such high-energy electrons may, indeed, be produced by argon ions of some keV.[28] None of the approaches enumerated above seemed to be adequate to describe, in a reasonable period of time, the transport phenomena in the MIM structure. Hence, taking into account the statistical nature of the scattering processes, we employed for this purpose a Monte Carlo method similar to that used by Ding and Shimizu.[29]

In this section, we introduce the basic assumptions of the underlying model. The Monte Carlo code itself closely follows the approach described in very detail in Ref. 29 and will not be reproduced in this paper. It should be only noted

that the simulation has been performed by assuming 10^7-10^9 electrons in the initial excitation, which provided a fairly good statistics at a moderate computation time.

The ion-induced electron emission in metal-insulator-metal (MIM) structures may be viewed as a three-step process: electron excitation and transport in the top metal layer and electron detection in the bottom-metal layer (internal emission) or in the vacuum (external emission). However, only the last two steps were simulated by the Monte Carlo code, while for the first step, simplifying assumptions have been made, as shown in the following.

A. Electron excitation

In a purely classical approach, the electronic excitation produced by the impinging argon ions is completely described if momentum $\hbar\mathbf{k}$ and position $\mathbf{r}$ of each excited electron were exactly determined at all times. The excitation can, thus, be characterized by a distribution function $f[\mathbf{k(t)},\mathbf{r(t)}]$, whose time evolution can be determined within the Monte Carlo simulation when knowing $f[\mathbf{k(0)},\mathbf{r(0)}]$.

In the following, we will introduce two excitation models: (i) a "surface excitation model," where we assumed that the projectile dissipates its entire kinetic energy at the surface of the silver film, and (ii) a "bulk excitation model," where we defined a depth profile of the dissipated energy on the basis of SRIM calculations.

1. Surface excitation model

Besides the main assumption of the model, i.e., that the electrons are excited only at the surface ($z=0$), we also assume that all electrons are excited at the moment $t=0$. This latter assumption has no effect on the computed yields, these being obtained by counting the electrons which succeed, regardless of their traveling time, to overcome the internal or the external potential barrier, respectively. Considering the lateral dimensions of the silver film to be infinite, the electron position at each time t in the xy plane plays no role in the simulation. As a consequence, $\mathbf{r}$ is completely determined by the depth coordinate z, while $\hbar\mathbf{k}$ can be expressed by means of the spherical coordinates ($\hbar k$, θ, ϕ). Here, $\hbar k$ is the absolute value of the momentum, θ is the polar angle, and ϕ is the azimuthal angle.

Now, by taking into account the parabolic relation $E=\hbar^2k^2/2m_e$, with m_e being the mass of the free electron, we employed the energy E as a variable parameter instead of the momentum $\hbar k$. Thus, by introducing the distribution function $f(E,\theta,\phi)$, we defined the probability

$$d^2p(E,\theta,\phi)=f(E,\theta,\phi)dEd\Omega \tag{1}$$

to excite an electron to an energy between E and $E+dE$ above the Fermi level, in a solid angle between Ω and $\Omega+d\Omega$. Considering the angular distribution of the excited electrons to be independent of their distribution in energies, f can be written as $f(E,\theta,\phi)=f_1(E)f_2(\theta,\phi)$, i.e., as the product of an energy distribution function (EDF) f_1 and an angular distribution function (ADF) f_2. Equation (1) may then be split into

$$dp_1(E)=f_1(E)dE \tag{2}$$

and

$$dp_2(\theta,\phi)=f_2(\theta,\phi)d\Omega. \tag{3}$$

Energy distribution function. A rough but not quite unrealistic model of energy distribution function is one of the type

$$f_1(E)=f_1(0)e^{-\beta E}. \tag{4}$$

Such a relation was employed also by Sroubek[30] and is consistent with recent calculations[31] which show a Fermi-like energy distribution already 15 fs after "ion impact," even though a thermalization due to electron-electron interaction was not considered. For convenience, we define an "electron temperature" T as $\beta=1/k_BT$ in Eq. (4) instead of the slope parameter β. The factor $f_1(0)$ can be obtained by normalizing Eq. (4),

$$\int_0^\infty f_1(E)dE=1. \tag{5}$$

Thus, the normalized EDF can be written as

$$f_1(E)=(1/k_BT)e^{-E/k_BT}. \tag{6}$$

A theoretical relationship between kinetic energy and temperature was established by Sroubek *et al.*[32] within a diffusion equation for atoms in solids. Thus, for the particular system Na^+-Cu, the electron temperature corresponding to a kinetic energy of 300–6000 eV ranges from 8000 to 35 000 K. Accordingly, we choose the temperature range for our simulation from 10 000 to 35 000 K.

Angular distribution function. The angular distribution of the excited electrons is closely related to the (an)isotropy of the excitation process. Therefore, we will examine the following two situations:

Isotropic excitation. This case applies to excitation processes where no momentum is transferred to the excited electrons as, for instance, in Auger processes. Hence, the ADF is independent of the polar emission angle θ and on the azimuthal emission angle ϕ being simply given by

$$f_2(\theta,\phi)=1/4\pi. \tag{7}$$

Anisotropic excitation. This case applies to excitation processes where, besides energy, also momentum is transferred to the electrons. This happens, for example, in binary collisions between projectile and target atoms ("promotion") or electrons ("friction"). The electron gains here a momentum $m_e\Delta v_x$ in the forward direction of the projectile. The anisotropy can be calculated in closed form. One complication arises, however, from the fact that the ADF and the EDF are not independent anymore. On the other hand, for our Monte Carlo simulation, it is more convenient to quantify the anisotropy by applying following conversion relations:

$$E'=E(1+2a\cos\theta+a^2), \tag{8}$$

$$\tan \theta' = \frac{\tan \theta}{1 + a/\cos \theta}, \tag{9}$$

where E' and θ' are the energy and the polar angle of the electron due to anisotropy, E and θ are the energy and the polar angle of the electron in the absence of anisotropy, and a is an anisotropy factor defined as $a = \Delta v_x / v$, with v the velocity of the excited electron in the absence of anisotropy. The anisotropy of the excitation is, hence, closely related to the kinetic energy of the projectile, E_{kin}. Therefore, we need to find the relation connecting E_{kin} with the electron temperature T. This can be established within the "bulk excitation model" described below.

2. Bulk excitation model

In this model, electrons are being excited not only at the surface of the metal film, but also deeper inside. Thus, in order to characterize the electronic excitation, we introduce, besides the energy E and the solid angle Ω, also the depth coordinate z. The probability to excite an electron in a depth between z and $z+dz$ to an energy between E and $E+dE$ above the Fermi level and in a solid angle between Ω and $\Omega+d\Omega$ is

$$d^3p(E,z,\theta,\phi) = f(E,z,\theta,\phi)dEdzd\Omega. \tag{10}$$

Assuming that the angular distribution of the excited electrons is independent of their distribution in energies and depths, the distribution function f can be split into an ADF and a z-dependent EDF, i.e., $f(E,z,\theta,\phi) = f_1(E,z)f_2(\theta,\phi)$.

Energy distribution function. We assume again an exponential EDF

$$f_1(E,z) = f_1(0,z)\exp\left(-\frac{E}{k_B T(z)}\right), \tag{11}$$

which depends implicitly on z via the electron temperature T. The factor $f_1(0,z)$ can be obtained by normalizing Eq. (11),

$$\int_0^\infty \int_0^\infty f_1(E,z)dEdz = 1, \tag{12}$$

which results in

$$f_1(0,z) = \left[k_B \int_0^\infty T(z)dz\right]^{-1}. \tag{13}$$

On the other hand, $f_1(0,z)$ can be related to the density of states at the Fermi level, $g(E_F)$, via

$$f_1(0,z) = \frac{g(E_F)S_0(z)}{N_e}, \tag{14}$$

where N_e is the total number of electrons excited in the metal film, while $S_0(z)$ may be viewed as an excitation cross section, which we will consider in the following to be a constant S_0. The equation system (13) and (14) leads to

$$N_e = g(E_F)S_0 k_B \int_0^\infty T(z)dz. \tag{15}$$

The depth profile of the electron temperature, $T(z)$, is related to the depth profile of the energy transferred by the projectile

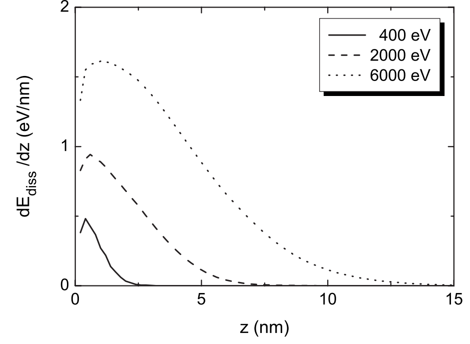

FIG. 2. Depth profile of the kinetic energy dissipated into the electronic system per unit path length as simulated with SRIM (Ref. 33) for selected ion kinetic energies. The energy dissipated by recoils is not included.

to the electronic system, which can be defined as

$$\frac{dE_{diss}(z)}{dz} = N_e \int_0^\infty E f_1(E,z)dE = g(E_F)S_0[k_B T(z)]^2. \tag{16}$$

An approximate expression for dE_{diss}/dz may be inferred from SRIM (Ref. 33) simulations. Figure 2 illustrates the depth profile of dE_{diss}/dz for kinetic energies of 0.4, 2, and 6 keV. Hereby, dissipated energy due to recoils was not considered. One may note that at 0.4 keV, the projectiles lose their kinetic energy within the first 3 nm, at 2 keV, the energy is dissipated in the electronic system entirely in the upper half of the silver film, while at 6 keV almost 15% of the total amount is dissipated in the lower half of the silver film. Obviously, dE_{diss}/dz depends also on the initial kinetic energy of the projectile, E_{kin}. Therefore, we have parametrized the dissipated energy as a function of z and E_{kin} by calculating the depth dissipation profiles for several kinetic energies between 400 and 6000 eV and by fitting each of them with a Gauss function centered at $z=0$ nm. Finally, we achieved for our particular Ar-Ag system the following expression:

$$\frac{dE_{diss}}{dz}(z) = \frac{dE_{diss}}{dz}(0)\exp\left(-2\frac{z^2}{w^2}\right), \tag{17}$$

with

$$(dE_{diss}/dz)(0) = 2.2E_{kin}^{0.5} \tag{18}$$

and

$$w = E_{kin}^{0.56}/15.5, \tag{19}$$

where w and z are given in nm while E_{diss} and E_{kin} are given in eV.

From the Eqs. (16) and (17), one may determine the locally defined temperature $T(z)$ as

$$T(z) = T(0)\exp\left(-\frac{z^2}{w^2}\right), \tag{20}$$

where

$$T(0) = \alpha_1 E_{kin}^{1/4} \tag{21}$$

is the electron temperature at the surface. Here, $\alpha_1 \approx 3580 S_0^{-1/2}$ is a proportionality factor, with T given in K, E_{kin} in eV, and S_0 in nm^2.

Equation (20) completely determines the distribution in depth and over energies of the excited electrons in the Ag film. Since the integral in Eq. (15) can now be calculated exactly, one can determine N_e as

$$N_e = g(E_F) S_0 k_B T(0) w \sqrt{\pi}/2 = \alpha_2 E_{kin}^{0.81}, \tag{22}$$

with $\alpha_2 \approx 0.41 S_0^{1/2}$, where E_{kin} is given in eV and S_0 in nm^2. The dimensions of the numerical constants in the Eqs. (18)–(22) are such that dE_{diss}/dz, w, $T(0)$, and N_e have the proper dimensions.

Angular distribution function. The bulk excitation model includes only the case of isotropic excitation, with the ADF given by Eq. (7). The second case of anisotropic excitation would be difficult to handle. On the other hand, since the projectile scatters several times with the lattice until it completely looses its energy, each scattering process leading to a change in direction, the excitation becomes more and more isotropic.

B. Electron transport

The transport of electrons in the metal is greatly affected by scattering on electrons, phonons, and defects. In order to model the transport of excited electrons, these were treated as classical particles, each following a certain trajectory in the metal film, while the target was considered to be free of defects. In our model, the trajectory of an excited electron is completely determined by (inelastic) electron-electron and (quasielastic) electron-phonon scattering processes. The former process is accompanied by momentum and energy transfer. In the latter process, only momentum transfer will be considered since the energy loss due to the excitation of longitudinal phonons, being of only some meV, can be neglected. The inelastic scattering represents, hence, the main loss channel of the excitation, while the elastic scattering is mainly responsible for the backscattering observed in electron spectroscopy experiments and is expected to drive an initially forward peaked electron distribution more isotropic.

1. Ballistic transport

The probability for ballistic transport, i.e., the probability that an electron excited at the surface, to an excess energy E with respect to the Fermi level, and a momentum $\hbar\mathbf{k}$ which makes an angle θ with the z axis (perpendicular to the surface), reaches the metal-oxide interface situated at a distance d without change in energy and momentum, can be written as

$$p_b(E,\theta) = \exp[-d/\lambda(E)\cos\theta], \tag{23}$$

where $\lambda(E)$ is the MFP of the electron in the metal. According to Matthiessen's rule, the transport MFP is given by

$$1/\lambda = 1/\lambda_i + 1/\lambda_e, \tag{24}$$

where λ_i and λ_e are the inelastic and the elastic MFPs, respectively. According to Eq. (1), a fraction

$$\gamma_b = \frac{1}{4\pi}\int_0^\infty \int_0^{\pi/2} \int_0^{2\pi} p_b(E,\theta) f(E,\theta,\phi) \sin\theta \, dE\, d\theta\, d\phi \tag{25}$$

of the initially excited electrons will reach the metal-oxide interface without being scattered. Besides ballistic electrons, also primary-excited electrons which undergo several scattering processes can be detected. Such electrons may also be included in an analytical model as shown by Kadlec[34] in his theory of internal photoemission. One disadvantage of this approach is that it includes only electrons which escape after at most two scattering processes, while electrons undergoing more than two scattering processes are neglected. Another problem is that even the consideration of two scattering processes leads to very complicated formulas. In addition, no electrons excited during inelastic electron-electron scattering processes (secondary electrons) are taken into account. Such kind of problems can be overcome with a Monte Carlo simulation.

The Monte Carlo method proposed by Ding and Shimizu[29] allows to follow each electron along its trajectory. In order to construct the trajectory of an electron, one needs to know the distance Δr the electron travels between two scattering events and the changes in energy and momentum, ΔE and $\Delta\hbar\mathbf{k}$, respectively, due to scattering.

2. Inelastic scattering

The differential cross section (DCS) for inelastic electron scattering is given by[35,36]

$$\frac{d^2\lambda_i^{-1}}{d(\hbar\omega)dq} = \frac{1}{\pi a_0 q E}\Im\left\{-\frac{1}{\epsilon(q,\omega)}\right\}, \tag{26}$$

where a_0 is the Bohr radius, $\hbar\omega$ is the energy loss, $\hbar q$ is the momentum transfer, E is the kinetic energy of the electron, $\epsilon(q,\omega)$ is the dielectric function of the solid, and λ_i is the electron inelastic mean-free path (IMFP). The energy-loss function, defined as the Fourier transform of the dielectric function $\Im\{-\frac{1}{\epsilon(q,\omega)}\}$, completely determines the probability of an inelastic-scattering event, the energy-loss distribution, and the scattering angular distribution.

Equation (26) may be written also with respect to the energy loss $\Delta E = \hbar\omega$ and the solid angle Ω by transforming variable q to θ. Thus, by applying the energy and momentum conservation laws, one may write

$$\frac{(\hbar q)^2}{2m_e} = 2E - \Delta E - 2\sqrt{E(E-\Delta E)}\cos\theta, \tag{27}$$

with m_e being the electron mass. The inelastic DCS is then given by

$$\frac{d^2\lambda_i^{-1}}{d(\Delta E)d\Omega} = \frac{1}{(\pi a_0 e)^2 q^2 E}\Im\left\{-\frac{1}{\epsilon(q,\omega)}\right\}\sqrt{E(E-\Delta E)}. \tag{28}$$

However, the energy-loss function is known (from optical and electron energy- loss experiments) only for $q=0$. In order to determine the wave vector- and frequency-dependent

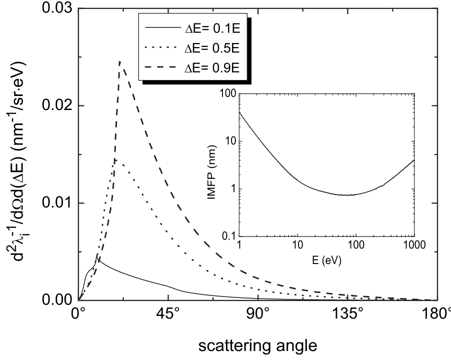

FIG. 3. Inelastic differential cross section plotted as a function of the scattering angle for electron energies of 5, 20, and 100 eV. In the inset, the energy dependence of the inelastic mean-free path used in our Monte Carlo simulation is shown.

energy-loss function, we applied the statistical approach of Penn[37] who proposed the following expansion scheme:

$$\Im\left\{-\frac{1}{\epsilon(q,\omega)}\right\} = \int_0^{\infty} d\omega_p G(\omega_p)\Im\left\{-\frac{1}{\epsilon_L(q,\omega,\omega_p)}\right\}, \quad (29)$$

where $\epsilon_L(q,\omega,\omega_p)$ is the longitudinal part of the Lindhard dielectric function and the plasma frequency ω_p is defined as

$$\omega_p(r) = \left(\frac{4\pi e^2}{m_e} n(r)\right)^{1/2}, \quad (30)$$

with $n(r)$ being a pseudo-charge-density introduced by Penn[37] as a part of his statistical approximation approach to ensure that

$$\Im\left\{-\frac{1}{\epsilon(0,\omega)}\right\} = \Im\left\{-\frac{1}{\epsilon(\omega)}\right\} \quad (31)$$

and $G(\omega)$ is a weight factor determined from the condition (31) to be

$$G(\omega) = \frac{2}{\pi\omega}\Im\left\{-\frac{1}{\epsilon(\omega)}\right\}. \quad (32)$$

Thus, a knowledge of the optical dielectric function $\epsilon(\omega)$ is sufficient to obtain $\Im\{-1/\epsilon(q,\omega)\}$ and, hence, the inelastic DCS and the IMFP.

The energy dependence of the inelastic DCS [as determined from Eq. (29)] is illustrated in Fig. 3 for energy losses (suffered by the electron due to scattering) of 10%, 50%, and 90% of the electron energy. The angle for the maximum scattering probability increases from 10° to 20° with increasing energy loss, meaning that forward scattering is more pronounced for low-energy losses. The energy dependence of the IMFP is shown in the inset of Fig. 3. While at 1 eV the IMFP is about 40 nm, it shows a strong decrease with increasing energy up to about 20 eV, exhibits then a minimum of 0.7 nm at about 70 eV, and rises than slightly, reaching a value of 4 nm at 1000 eV. This curve is in good agreement with the Fermi-liquid theory at low energies as well as with the empiric data of Seah and Dench.[27]

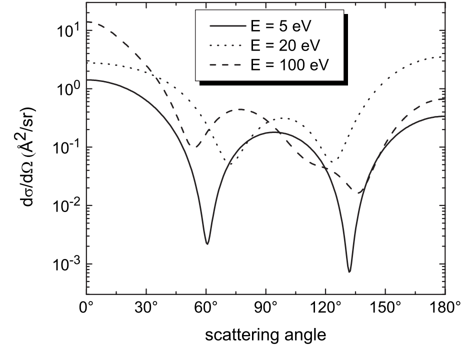

FIG. 4. Elastic differential cross section calculated from the Mott cross section as a function of the polar scattering angle for electron energies of 5, 20, and 100 eV.

3. Elastic scattering

In our simulation, we employed tabulated data[38] of Mott differential elastic cross sections[39] computed for electron energies between 5 and 30 000 eV. The calculations are based on the analytical approximation for the atomic electrostatic potential given by the Thomas-Fermi- Dirac model[40] and the numerical algorithm described in Ref. 41. Although the model neglects exchange and polarization effects, the computed data are believed[38] to describe qualitatively the elastic-scattering processes for electron energies of the order of 10 eV and higher, while for energies above 100 eV, data are in fairly good agreement with experimental values. In the absence of other reliable data on elastic cross sections, we applied for energies below 5 eV the cross-section values calculated for 5 eV. For energies above 5 eV, we determined the missing cross sections by spline interpolation of the tabulated data. A further assumption of our model is that the electron loses no energy during an elastic-scattering process.

Figure 4 illustrates the differential elastic cross sections $d\sigma_e/d\Omega$ for electrons of 5, 20, and 100 eV excess energy, respectively, traveling through a silver target. One may observe a similar qualitative behavior at different energies, absolute cross-section values strongly vary, however, with energy as well as with the scattering polar angle θ. We determined not tabulated cross sections by spline interpolation, while for energies below 5 eV, we applied the cross-section values calculated for 5 eV.

In Ref. 29, the elastic mean-free path (EMFP) λ_e of the electrons was determined from the total cross section σ_e by the formula

$$\lambda_e^{-1} = \frac{N_A\rho}{A}\sigma_e, \quad (33)$$

with N_A being the Avogadro's number, ρ the silver density, and A the silver mass number. According to Eq. (33), the EMFP shows almost no energy dependence in the energy range between 20 and 100 eV, amounting to about 0.2 nm, while below 10 eV, it goes through a minimum of 0.07 nm at 10 eV and reaches 0.8 nm at 5 eV. At very low energies, the EMFP should approach the conductivity mean-free path of bulk silver. This can be estimated within the Drude model by taking into account the Drude relaxation time at 273 K (Eq.

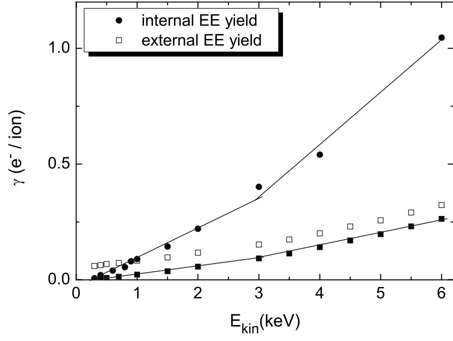

FIG. 5. Total internal (full circles) and external (empty squares) electron emission yields, γ_i and γ_e, respectively, induced by singly-charged argon ions in a Ag-AlO_x-Al junction, under normal incidence, vs kinetic impact energy of the ions. Kinetic EE yields (full squares) assuming a constant potential EE yield of 0.06.

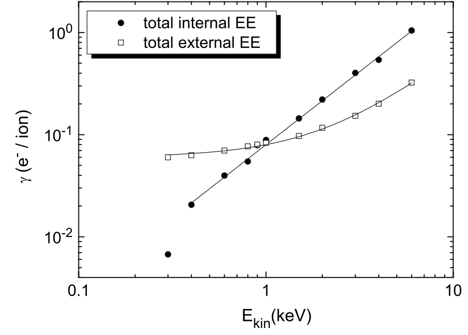

FIG. 6. Double logarithmic representation of the total internal and external electron emission yields plotted in Fig. 5.

42) to be about 40 nm. This is consistent with EMFP values derived for Au from BEEM measurements at electron energies between 0.5 and 1.5 eV.[25] Since no experimental EMFP data are available in the energy range below 100 eV, we partly employed the same assumption as other authors did in their Monte Carlo simulations,[43,44] namely, that $\lambda_e=10$ nm in the whole energy range. Since most of the kinetically excited electrons have excess energies of a few eV, we believe this to be a reasonable assumption. We will, however, discuss later in this paper (see Sec. V B 1) also the influence of λ_e on the electron yields.

C. Electron emission

An excited electron is considered to be internally or externally emitted if the electron succeeds to pass the internal or the external potential barrier, respectively. Thereby, we took into account the quantum-mechanical refraction of the electrons at the barrier. The probability that an electron, reaching the potential barrier with an energy E, under an angle θ with the surface normal, passes the barrier is given by the expression[45]

$$\mathrm{Tr}(E,\theta)=\begin{cases}\dfrac{4\sqrt{1-t(E,\theta)}}{[1+\sqrt{1-t(E,\theta)}]^2}, & \text{if } t(E,\theta)<1\\ 0, & \text{otherwise,}\end{cases} \tag{34}$$

where $t(E,\theta)=W/(E\cos^2\theta)$. Here, W is either the internal barrier height W_i, which we estimated from photo-emission experiments to be about 2 eV, or the external barrier height W_e of about 4.3 eV (Ref. 46) (average value of literature data on polycrystalline silver).

IV. RESULTS

In Fig. 5, the measured internal EE yield γ_i and the external EE yield γ_e are plotted against the kinetic impact energy E_{kin} of the argon ions in the energy range of 0.3–6 keV. One may note that γ_i increases from 0.006 at 300 eV to 1.1 at 6 keV, while γ_e reaches only 0.32 at 6 keV. This latter value is consistent with experimental data found in the literature.[47] Another major difference between the two data sets is that γ_e varies only slightly below 1 keV and seems to saturate at a value close to 0.06, while γ_i drops faster and almost vanishes at 300 eV. The observed energy dependence of γ_e is in a good qualitative agreement with that observed in similar experiments[48] on external emission. Each of the two data plots may be roughly fitted by two straight lines with different slopes, which intersect at about 3 keV (see Fig. 5).

Such a change of the slope was observed before on some other target projectile systems,[49,50] though a systematics on this was found neither with projectile nor with target. Let us denote in the following the region below 3 keV as the *low-energy* region and the region above 3 keV as the *high-energy* region. No saturation effect is observed in the internal EE toward low energies, where the linear fit cuts the abscissa at about 240 eV, suggesting the existence of a threshold energy for internal EE and, at the same time, the absence of any significant contribution from PEE.

Interestingly, in the double-logarithmic representation shown in Fig. 6, log γ_i seems to scale with log E_{kin} as

$$\log \gamma_i = \alpha_i + \beta_i \log E_{kin}, \tag{35}$$

suggesting a power-law scaling

$$\gamma_i = (E_{kin}/\epsilon_i)^{\beta_i}, \tag{36}$$

with the fit parameters $\alpha_i=-5.4$, $\epsilon_i=6000$ eV, and $\beta_i=1.43$. In Fig. 6, we fitted the external EE yield also by a power-law function, but this time of the type

$$\gamma_e = \gamma_e^0 + (E_{kin}/\epsilon_e)^{\beta_e} \tag{37}$$

by assuming $\gamma_e^0=0.06$. The best fit is obtained for $\epsilon_e \approx 16\,000$ eV and $\beta_e \approx 1.4$. Equation (37) suggests, hence, the existence of two contributions to the external emission yield: the PEE yield $\gamma_e^{\mathrm{PEE}}=0.06$ and the KEE yield $\gamma_e^{\mathrm{KEE}} \propto E_{kin}^{1.4}$. From Eq. (36), it is evident that the potential energy gives practically no contribution to the internal emission yield. A further interesting observation is that the internal KEE yield, γ_i^{KEE}, also approximately scales as $E_{kin}^{1.4}$. This indicates that the ratio $\gamma_i^{\mathrm{KEE}}/\gamma_e^{\mathrm{KEE}}$ is practically constant and equal to about 4.

V. DISCUSSION

A. PEE

A singly-charged ion is known to dissipate its potential (ionization) energy within an Auger neutralization process, in which the interaction of two conduction electrons causes one electron to neutralize the ion in the ground state and the other to be excited above the Fermi level of the metal.[6] Argon ions carrying a potential energy $E_{pot}=15.7$ eV may excite electrons with an excess energy above the Fermi level E_F of at most $E_{pot}-\Phi$,[6] where Φ is the work function of the metal surface, which amounts to 4.3 eV (Ref. 46) in the case of silver. The external EE yield of 0.06 suggests that at least 6% of the excited electrons have energies between 4.3 and 11.3 eV and are directed toward the surface.

The contribution of the potential energy to the external EE yield has been quantified by Kishinevskii,[51] who gave the semiempirical formula

$$\gamma_e^{PEE} = \frac{0.2}{E_F}(0.8E_{pot} - 2\Phi), \tag{38}$$

where E_F is the Fermi energy of the metal, E_{pot} is the potential energy of the projectile, and Φ is the work function of the metal. Assuming $E_F=5.5$ eV (Ref. 52) (corresponding to a free-electron gas), $E_{pot}=15.7$ eV,[53] and $\Phi=4.3$ eV, this gives a value of about 0.15 for the external PEE yield, which is in a fairly good agreement with the experimental value of 0.06, in spite of the simplicity of the model.

As shown in the previous section, if there is a contribution of the potential energy to the internal EE yield, it is much smaller than that of the kinetic energy. Qualitatively, this can be explained as follows. Because no kinetic momentum is expected to be transferred in the Auger neutralization process, the induced electron emission is believed to be isotropic. As a consequence, excited electrons are equally directed toward the metal-oxide interface and toward the metal-vacuum interface. In addition, the ion-neutralization process occurs at or close to the metal surface. As a consequence, the excited electrons should more easily escape into the vacuum then into the bottom-metal layer of the MIM structure, since, in the latter case, electrons have to cover a distance of ≈ 15 nm. The probability of an excited electron to reach the metal-oxide interface without energy loss (ballistic transport) is at most $\exp(-d_{Ag}/\lambda_e)$, where $d_{Ag}=15$ nm is the thickness of the silver film and λ_e is the IMFP of the electrons. The IMFP of an electron with an excess energy of about 10 eV is known to be of the order of 1 nm.[37] The chance that such a "high-energy" electron would reach the interface would be as low as $\approx 1:10^6$. The IMFP increases with decreasing electron energy, being as high as 100 nm at 1 eV.[54] Such an electron would, however, not be able to pass the internal barrier with a height of about 2 eV. For the energy range of interest, i.e., between 2.0 and 11.4 eV, the Fermi-liquid theory predicts[26] IMFPs in the range of 1–10 nm.

B. KEE

While an Ar^+ ion dissipates only 15.7 eV of potential energy into the electronic system, it is expected that it dissipates a larger amount of kinetic energy. By means of the simulation program SRIM2006,[33] one can estimate that about 6% of its kinetic energy, i.e., 18–360 eV in our case, is dissipated directly into the electronic system of the silver film by *electronic stopping*. Also, a few percent of the ion kinetic energy is dissipated indirectly by the recoil atoms resulting from collisions of the Ar ion with the target atoms. Ion kinetic energy is not transferred to a single electron, as the potential energy, but it leads to the excitation of several electrons along the trajectory of the projectile. Assuming a Fermi-like energy distribution of the excited electrons, most of these electrons are of low-energy and, hence, not able to pass the potential barrier. As a consequence, much more kinetic energy is to be dissipated in order to induce the same EE yield as in the PEE. This is confirmed by the experimental data (see Fig. 5) which show that the external KEE yield equals the external PEE yield only when the kinetic energy is raised to about 2 keV.

The external KEE yield, obtained by subtracting the PEE contribution γ_e^{pot} from the total external yield, is lower than the internal KEE yield over the whole energy range between 0.3 and 6.0 keV, provided that $\gamma_e^{pot}=0.06$ and $\gamma_i^{pot}=0$ (see Fig. 5). Let us assume in a gedanken experiment an isotropic distribution of excited electrons. Then, one half of them would be directed toward the surface, while the second half would be directed toward the metal-oxide interface. Supposing that electrons move in the metal without being scattered (ballistic transport), more electrons will pass the internal barrier ($W_i \approx 2$ eV) than the external one [$W_e=4.3$ eV (Ref. 46] and, hence, the ratio γ_i/γ_e would always be greater than 1. Electron-electron and electron-phonon scattering processes are, however, not negligible and cause energy loss and change of momentum. Scattered electrons are, thus, deviated from their initial direction and additionally may have not enough energy to pass the barrier. But even in elastic collisions with the ion cores of the metal film, where electrons will loose only a negligible amount of energy, electrons may be prevented to reach the internal barrier, being instead scattered back and eventually detected as external electrons. Such scattering events are, thus, expected to reduce the internal emission yield γ_i and, hence, the ratio γ_i/γ_e. The reduction of γ_i due to scattering is thereby expected to be the stronger the thicker the silver film is.

In order to perform a more quantitative analysis of the emission process, we developed a computer simulation program based on the MC method described in Sec. III. Thereby, we defined two excitation models: the surface excitation (SE) model (see Sec. III A 1) and the bulk excitation (BE) model (see Sec. III A 2). One of the shortcomings of the former model is that it does not provide a relation between the ion kinetic energy E_{kin} and the electronic temperature at the metal surface $T(z=0)$, while the latter does. In order to enable a comparison of the results obtained by the two excitation models, we will assume also in the SE model the relation between E_{kin} and $T(0)$ given in Eq. (21). This depends, however, on the parameter S_0 defined in Eq. (14), which is not known. To estimate S_0, we proceeded as follows. We run the MC simulation by varying $T(0)$, keeping E_{kin} constant at 6 keV. Then we compared the computed external EE yield to the experimental one and found the best

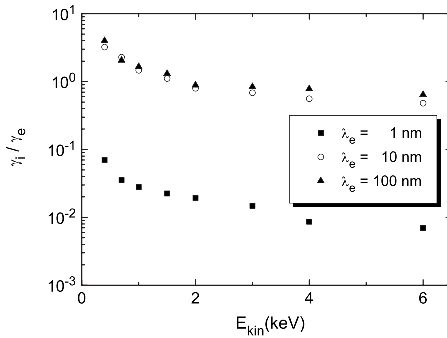

FIG. 7. Ratio of internal to external EE yield computed, within the surface excitation model, as a function of the kinetic energy, for selected elastic mean-free paths, by assuming an isotropic distribution function of the excited electrons.

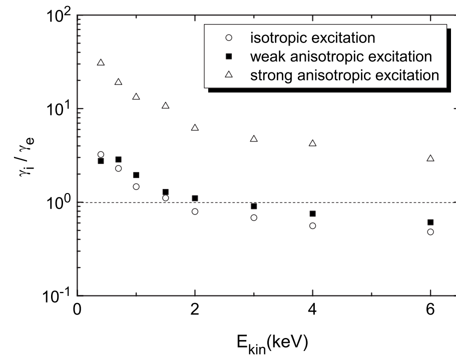

FIG. 8. Ratio of internal to external EE yield computed, within the surface excitation model, as a function of the kinetic energy for an isotropic and two anisotropic distribution functions of the excited electrons.

match for $T(0) \approx 17\,700$ K. From Eq. (21), we found that $\alpha_1 \approx 2000$ K/eV$^{1/4}$ and $S_0 \approx 3.16$ nm^2. The latter corresponds to the area of a circle with a radius of 1 nm. In the following, we will compute the EE yields and analyze the influence of the excitation properties (e.g., anisotropy) as well as of the device properties (e.g., internal barrier height, film thickness) upon them.

1. Influence of elastic scattering

For a qualitative study on the influence of the scattering processes on the emission yields, we performed a Monte Carlo simulation based on the SE model described in Sec. III A 1. From Fig. 7, it is apparent that the computed yields ratio is also very sensitive to the choice of the EMFP, especially when the EMFP λ_e is chosen to be much smaller than the film thickness. Thus, for $\lambda_e = 1$ nm, the external yield is 1–2 orders of magnitude larger then the internal one. Obviously, the very short EMFP is related to a high rate of elastic-scattering events, which strongly inhibits the transport of the electrons through the metal and, hence, reduces the internal emission. In contrary, for $\lambda_e \gg d_{\mathrm{Ag}}$, the ratio tends to saturate, since elastic-scattering events are very seldom and the electron-electron scattering becomes the dominant loss channel. A further observation is that the qualitative energy dependence seems to be less affected by the choice of the EMFP value.

2. Influence of the excitation anisotropy

Depending on the particular excitation mechanism, not only energy, but also momentum may be transferred by the ion to the electronic system. This may introduce an anisotropy of the electronic excitation, which would be favorable to the internal emission. We examined the effect of this anisotropy on the yield ratio γ_i / γ_e by considering following two excitation mechanisms:

(a) Electronic friction. This mechanism implies a direct interaction of the projectile with the electronic system. In a classical picture, the energy is transferred via a binary collision between projectile and a free electron from the conduction band. In this case, besides energy, also momentum is transferred to the electron, the velocity gain in the direction of the projectile being equal to twice the velocity of the projectile, i.e., $\Delta v_x = 2v_0$. This determines then the anisotropy factor in Eqs. (8) and (9). In the following, we will refer to this case as the *strong anisotropic excitation*.

(b) Electron promotion. This mechanism is known to occur in inner-shell excitation processes due to close binary encounters between projectile and target atoms. The core holes excited during collisions are, however, not mobile, decaying in fast Auger processes which finally lead to the excitation of conduction electrons. The ADF of the electrons excited in this promotion mechanism can be considered as being isotropic in the center-of-mass system of the colliding atoms. In this case, the anisotropy of the ADF resides only from the fact that the excited electron gains a forward velocity $\Delta v_x = M_p / (M_p + M_t) v_0 \approx 0.27 v_0$ in the laboratory system, with M_p and M_t being the mass of the projectile and of the target atom, respectively. This case will be referred to as the *weak anisotropic excitation*.

Figure 8 depicts the yield ratio γ_i / γ_e as a function of the kinetic energy of the Ar ion, as determined by the MC simulation within the SE model, with the correspondence between surface temperature T and E_{kin} as determined within the BE model. It shows that the anisotropy induced by the *electronic friction* excitation mechanism strongly affects the ratio γ_i / γ_e, rising it, with respect to the isotropic case, by about 1 order of magnitude. However, although the electron promotion was suggested to be the main excitation mechanism in the case of light projectiles as H and He,[10] it is believed to be less efficient when heavy projectiles are involved due to the large difference in mass between projectile and electron. Recently, it was shown[55] that rather the *electron promotion* is the dominant excitation mechanism at low projectile velocities ($v < v_F$). The weak anisotropy induced by this mechanism has, however, a small influence upon the yield ratio when compared to the isotropic case, as can be seen in Fig. 8.

3. Influence of excitation depth

Since the Ar ion dissipates its kinetic energy not only at the surface but also along its trajectory inside the silver film, we applied the BE model described in Sec. III A 2 to calculate the contribution of the electrons excited in deeper atomic

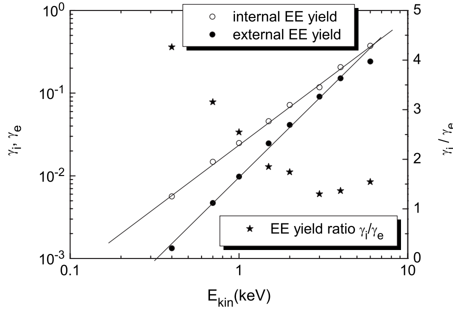

FIG. 9. Internal, external, and ratio of internal to external EE yield computed within the bulk excitation model as a function of the kinetic energy.

layers to the emission yields. Figure 9 depicts the absolute values of the internal and the external emission yield, γ_i and γ_e, respectively, as well as the ratio γ_i/γ_e as a function of the kinetic energy of the Ar ions. The most important observation is that the computed internal yield exceeds the external one over the whole energy range. Moreover, the MC simulation predicts the power-law scaling of the internal and the external EE yield as can immediately be inferred from Fig. 9 due to the double-logarithmic representation. Thus, γ_i can be well fitted by Eq. (36), with ϵ_i=11 500 eV and β_i=1.53, whereas for γ_e, the best power-law fit is obtained for ϵ_e =10 800 eV and β_e=1.96. The different β values indicate already that the computed yield ratio γ_i/γ_e clearly depends on kinetic energy. This is illustrated in Fig. 9, too. In comparison to the SE model, one may observe an increase of the yield ratio by a factor of about 2–3, this becoming in the BE model greater than unity over the whole energy range.

4. Influence of internal barrier height

The magnitude of the internal KEE yield is expected to depend also strongly on the potential barrier height, since the potential barrier makes a rigorous selection of the excited electrons, acting as a "high-pass" filter.[56] Figure 10 depicts the computed internal emission yield γ_i as a function of the kinetic energy for selected internal barrier heights W_i in the range of 1.6–2.2 eV. In all cases, the computed data can be well fitted by Eq. (36). It can be noticed that γ_i increases with decreasing W_i. This was expected since, by lowering

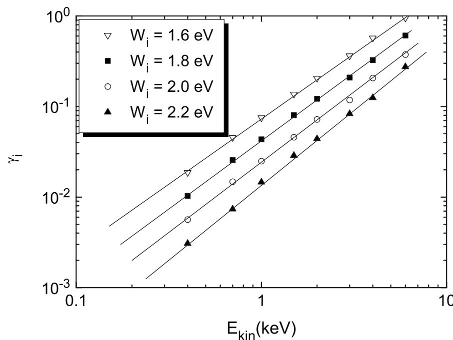

FIG. 10. Internal emission yields computed, within the bulk excitation model, as a function of the kinetic energy for selected values of the internal barrier height.

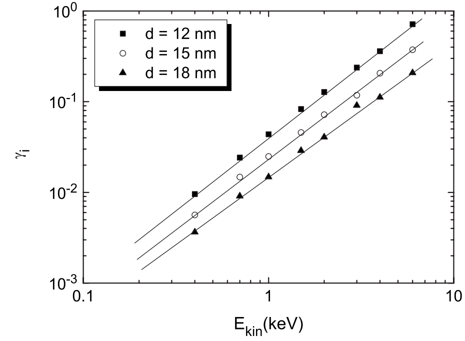

FIG. 11. Internal emission yields computed, within the bulk excitation model, as a function of the kinetic energy for selected values of the silver film thickness.

W_i, more excited electrons are able to overcome it. Thus, a lowering of the barrier by 10% leads to an increase of γ_i by more than 100%. By reducing the barrier height from 2.2 to 1.6 eV, the fitted parameters ϵ_i and β_i became also smaller. While ϵ_i varies from 13 600 to 6000 eV, β_i changes from 1.64 to 1.45. Interestingly, the computed yields at 1.6 eV are very close to the experimental values. This result is, however, rather fortuitous and should not lead to the conclusion that the internal barrier height is in fact 1.6 eV. Finally, it should be noted that the external emission yield is not influenced by the choice of W_i and, hence, the ratio γ_i/γ_e shows the same behavior with W_i as γ_i.

5. Influence of film thickness

Due to the fact that the ballistic transport of excited electrons toward the internal barrier is perturbed by elastic and inelastic processes, the internal emission yield γ_i will depend also on the thickness of the silver film d_{Ag}. Figure 11 shows how d_{Ag} influences the dependence of γ_i on E_{kin} when the EMFP is taken to be 10 nm. As expected, γ_i increases, at given E_{kin}, with decreasing d_{Ag}. Again, we could perform a quantitative analysis by fitting the computed data by means of Eq. (36). This shows that ϵ_i increases from 7500 to 16 500 eV when d_{Ag} increases from 12 to 18 nm. On the contrary, β_i decreases slightly, i.e., from 1.58 to 1.50 in the same thickness range. The latter observation is probably related to the fact that, in a thicker Ag film, an excited electron undergoes more scattering events and, hence, leads to the creation of more secondary electrons.

VI. CONCLUSIONS

In summary, we have investigated the electronic excitation induced by singly charged argon ions in the top 15 nm Ag film of a Ag-AlO_x-Al sandwich structure. The experiments revealed two interesting aspects. First, no significant contribution of the potential energy to the internal EE yield is observed. Second, the kinetic part of the internal electron emission yield γ_i seems to exceed the external one over the entire energy range investigated here, i.e., 0.4–6 keV, by factor of about 4.

A MC simulation method based on existent models of elastic and inelastic scattering in metal films has been devel-

oped in order to simulate the electron transport in the film and over the internal and the external potential barrier of the sandwich structure. Within the "surface excitation model," we found that the computed ratio $\gamma_i/\gamma_e < 1$ for kinetic energies $E_{kin} > 1500$ eV. For $E_{kin} < 1500$ eV, the ratio becomes greater then 1 and reaches a value of 4 at 0.4 keV provided that $\lambda_e \approx d_{\mathrm{Ag}}$. Yield ratios $\gamma_i/\gamma_e > 2$ were obtained within the surface excitation model by defining a so-called "strong anisotropic" distribution function of the excited electrons. This assumes that projectiles transfer energy and momentum directly into the electronic system, being, however, not very realistic due to the known inefficiency of such an excitation mechanism at low kinetic energies.

The experimental results are supported, however, by data computed within the "bulk excitation model" based on a depth profile of the energy dissipated into the electronic system estimated from SRIM (Ref. 33) calculations. We showed that, within the assumptions of the model, γ_i/γ_e is greater than unity over the whole energy range. Despite the roughness and simplicity of the underlying model, the MC simulation succeeds to describe well the dependence of γ_i on E_{kin}, predicting a power-law scaling similar to that found experimentally. Finally, we showed that the film thickness and internal barrier height W_i have a strong influence on the internal emission yield γ_i and, hence, on the yield ratio γ_i/γ_e, too. Thus, for lower values of d_{Ag} and W_i, the model predicts yield ratios which are even larger than those found in the experiment.

ACKNOWLEDGMENTS

This work was supported by the Deutsche Forschungsgemeinschaft within SFB616 "Energy dissipation at surfaces." Partial support by the Austrian FWF and the European ITS LEIF network is gratefully acknowledged.

[1] M. P. Villard, J. Phys. (Paris) **8**, 1 (1899).
[2] B. A. Brusilovsky, Appl. Phys. A: Mater. Sci. Process. **50**, 111 (1990).
[3] R. A. Baragiola, Nucl. Instrum. Methods Phys. Res. B **78**, 223 (1993).
[4] M. L. E. Oliphant and P. B. Moon, Proc. R. Soc. London, Ser. A **127**, 388 (1930).
[5] S. S. Shekhter, Zh. Eksp. Teor. Fiz. **7**, 750 (1937).
[6] H. D. Hagstrum, Phys. Rev. **96**, 336 (1954).
[7] E. S. Parilis and L. M. Kishinevsky, Sov. Phys. Solid State **3**, 885 (1960).
[8] O. B. Firsov, Sov. Phys. JETP **9**, 1076 (1959).
[9] E. V. Alonso, R. A. Baragiola, J. Ferrón, M. M. Jakas, and A. Oliva-Florio, Phys. Rev. B **22**, 80 (1980).
[10] R. A. Baragiola, E. V. Alonso, and A. Oliva Florio, Phys. Rev. B **19**, 121 (1979).
[11] G. Lakits, F. Aumayr, M. Heim, and H. Winter, Phys. Rev. A **42**, 5780 (1990).
[12] W. Heiland, H. G. Schäffler, and E. Taglauer, Surf. Sci. **35**, 381 (1973).
[13] H. Eder, W. Messerschmidt, H. Winter, and F. Aumayr, J. Appl. Phys. **87**, 8198 (2000).
[14] U. Fano and W. Lichten, Phys. Rev. Lett. **14**, 627 (1965).
[15] R. Baragiola, *Low Energy Ion-Surface Interactions* (Wiley, New York, 1994), Chap. 4.
[16] S. Meyer, D. Diesing, and A. Wucher, Phys. Rev. Lett. **93**, 137601 (2004).
[17] S. Meyer, D. Diesing, and A. Wucher, Nucl. Instrum. Methods Phys. Res. B **230**, 608 (2005).
[18] D. A. Kovacs, T. Peters, C. Haake, M. Schleberger, A. Wucher, A. Golczewski, F. Aumayr, and D. Diesing, Phys. Rev. B **77**, 245432 (2008).
[19] T. Peters, C. Haake, D. Diesing, D. A. Kovacs, A. Golczewski, G. Kowarik, F. Aumayr, A. Wucher, and M. Schleberger, New J. Phys. **10**, 073019 (2008).
[20] D. Diesing, A. W. Hassel, and M. M. Lohrengel, Thin Solid Films **342**, 282 (1999).
[21] Y. Jeliazova, M. Kayser, B. Mildner, A. W. Hassel, and D. Diesing, Thin Solid Films **500**, 330 (2006).
[22] E. Galutschek, R. Trassl, E. Salzborn, F. Aumayr, and H. Winter, J. Phys.: Conf. Ser. **58**, 395 (2007).
[23] G. Kowarik, M. Brunmayr, and F. Aumayr, Nucl. Instrum. Methods Phys. Res. B **267**, 2634 (2009).
[24] J. Schou, Phys. Rev. B **22**, 2141 (1980).
[25] L. D. Bell, Phys. Rev. Lett. **77**, 3893 (1996).
[26] J. J. Quinn, Phys. Rev. **126**, 1453 (1962).
[27] M. P. Seah and W. A. Dench, Surf. Interface Anal. **1**, 2 (1979).
[28] C. Benazeth, N. Benazeth, and L. Viel, Surf. Sci. **78**, 625 (1978).
[29] Z.-J. Ding and R. Shimizu, Scanning **18**, 92 (1996).
[30] Z. Šroubek, Phys. Rev. Lett. **78**, 3209 (1997).
[31] C. Race, D. Mason, and A. Sutton, J. Phys.: Condens. Matter **21**, 115702 (2009).
[32] Z. Šroubek, X. Chen, and J. A. Yarmoff, Phys. Rev. B **73**, 045427 (2006).
[33] A detailed description of the simulation program package SRIM2006 can be found at http://www.srim.org
[34] J. Kadlec, Phys. Rep. **26**, 69 (1976).
[35] P. Nozières and D. Pines, Phys. Rev. **113**, 1254 (1959).
[36] D. Pines and P. Nozieres, *The Theory of Quantum Fluids* (Benjamin, New York, 1966), Vol. 1.
[37] D. R. Penn, Phys. Rev. B **35**, 482 (1987).
[38] Computed data of differential and total elastic cross sections can be found on the website http://www.ioffe.ru
[39] N. F. Mott, Proc. R. Soc. London, Ser. A **124**, 425 (1929).
[40] R. A. Bonham and T. G. Strand, J. Chem. Phys. **39**, 2200 (1963).
[41] P. J. Bunyan and J. L. Schonfelder, Proc. Phys. Soc. London **85**, 455 (1965).
[42] N. W. Ashcroft and N. Mermin, *Solid State Physics* (Saunders, Philadelphia, 1976), Chap. 1, p. 10.
[43] J. Mooney and J. Silverman, IEEE Trans. Electron Devices **32**, 33 (1985).
[44] L. J. Schowalter and E. Y. Lee, Phys. Rev. B **43**, 9308 (1991).
[45] C. Cohen-Tannoudji, B. Diu, and F. Laloë, *Mecanique Quantique* (Hermann Editeurs des Sciences et des Arts, Paris, 1973),

p. 75.
[46] N. Ashcroft and N. Mermin, *Solid State Physics* (Saunders, Philadelphia, 1976), Chap. 18, p. 363.
[47] R. Baragiola, E. Alonso, J. Ferron, and A. Oliva-Florio, Surf. Sci. **90**, 240 (1979).
[48] K. Töglhofer, F. Aumayr, and H. Winter, Surf. Sci. **281**, 143 (1993).
[49] G. D. Magnuson and C. E. Carlston, Phys. Rev. **129**, 2403 (1963).
[50] S. N. Markin, D. Primetzhofer, S. Prusa, M. Brunmayr, G. Kowarik, F. Aumayr, and P. Bauer, Phys. Rev. B **78**, 195122 (2008).
[51] L. M. Kishinevsky, Radiat. Eff. **19**, 23 (1973).
[52] N. Ashcroft and N. Mermin, *Solid State Physics* (Saunders, Philadelphia, 1976), Chap. 2, p. 38.
[53] I. Velchev, W. Hogervorst, and W. Ubachs, J. Phys. B **32**, L511 (1999).
[54] C. R. Crowell and S. M. Sze, *Physics of Thin Films* (Academic Press Inc., New York, 1967), Vol. 4.
[55] A. Duvenbeck, O. Weingart, V. Buss, and A. Wucher, Nucl. Instrum. Methods Phys. Res. B **255**, 281 (2007).
[56] D. A. Kovacs, J. Winter, S. Meyer, A. Wucher, and D. Diesing, Phys. Rev. B **76**, 235408 (2007).